Visible-Light-Driven N−F−Codoped TiO_2 Photocatalysts. 1. Synthesis by Spray Pyrolysis and Surface Characterization

Di Li,* Hajime Haneda, Shunichi Hishita, and Naoki Ohashi

Advanced Materials Laboratory, National Institute for Materials Science (NIMS), 1-1 Namiki, Tsukuba, Ibaraki 305-0044, Japan

Received June 6, 2004. Revised Manuscript Received March 11, 2005

Novel photocatalytic materials, yellow-colored N−F-codoped TiO_2 (NFT) powders, were synthesized from a mixed aqueous solution containing $TiCl_4$ and NH_4F by spray pyrolysis (SP). The resulting powders were characterized by field-emission scanning electron microscopy (FE-SEM), X-ray diffraction (XRD), thermogravimetry-differential thermal analysis (TG-DTA), NH_3-temperature-programmed desorption (NH_3-TPD), X-ray photoelectron spectroscopy (XPS), and N_2 adsorption. FE-SEM images and N_2 adsorption confirm that the NFT powders possessed spherical particles with a highly porous surface morphology. The doped N and F concentrations in the NFT powders depended significantly on the SP temperature and ranged from 0.10 to 0.26 and from 0.11 to 0.40 atomic % (at. %), respectively. NH_3-TPD measurement indicates that the surface of the NFT powder was strongly acidic. Moreover, by investigating the characteristics of the TiO_2 precursor hydrolysis and the thermal decomposition behaviors of the other components in the starting solution, we elucidated the reasons for the formation of porous NFT powders, which we ascribed to the enormous gas evolution from NH_4F during TiO_2 particle formation and the template role played by NH_4Cl.

1. Introduction

Visible-light-driven photocatalytic technology has attracted much attention because it is a vital step in using solar energy to eliminate undesired chemical substances for environmental conservation and to split water for green-energy hydrogen production.[1−3] For the latter aim, the development of new photocatalytic materials seems to be a main research target in this field.[3] For the former aim, the photocatalytic materials have mainly focused on TiO_2 and ZnO semiconductors because of their high reactivity, low cost, and environmentally friendly features.[4,5] Their modification with the goal of improving their optical absorption and photocatalytic performances, e.g., extending spectral response into the visible region and enhancing photocatalytic activity, seems to be the most important interest.[6,7]

The simplest and most feasible TiO_2 modification approaches for achieving visible-light-driven photocatalysis seem to be N-doping, i.e., doping nitrogen atoms into substitutional sites in the crystal structure of TiO_2 (e.g., $TiO_{2-x}N_x$) by calcination in an NH_3 atmosphere or by a wet chemical route.[1,8−10] Other approaches, such as incorporating transition metal ions (e.g., V or Cr ions) by implantation and introducing oxygen vacancies by hydrogen plasma treatment, require expensive special equipment.[11,12] The presence of doped nitrogen extends the optical absorption of TiO_2 to the visible-light spectrum and enhances the visible-light-driven photocatalysis; however, the reactivity or quantum efficiency is still very low for practical applications. Increasing the photocatalytic activity is a big challenge in this research field. The introduction of new active sites into the N-doped TiO_2 system should be a promising approach for solving this problem.

Some researchers have reported that the introduction of fluorine atoms into a photocatalytic system is effective for enhancing the photocatalytic activity of TiO_2.[13−15] However, it should be noted that all of the photocatalytic reactions they targeted proceeded under UV irradiation. Achieving visible-light-driven photocatalysis seems to be difficult only through introducing fluorine atoms into TiO_2 because a great improvement in visible-light absorption was not observed

* Corresponding author. Tel.: +81-29-851-3354 ext. 8608. Fax: +81-29-855-1196. E-mail: LI.Di@nims.go.jp.

(1) Asahi, R.; Morikawa, T.; Ohwaki, T.; Aoki, K.; Taga, Y. *Science* **2001**, *392*, 269.
(2) Li, D.; Haneda, H. *J. Photochem. Photobiol. A: Chem.* **2003**, *155*, 171.
(3) Kasahara, A.; Nukumizu, K.; Hitoki, G.; Takada, T.; Kondo, J. N.; Hara, M.; Kobayashi, H.; Domen, K. *J. Phys. Chem. A* **2002**, *106*, 6750.
(4) Mills, A.; Hunte, S. L. *J. Photochem. Photobiol. A: Chem.* **1997**, *108*, 1.
(5) Li, D.; Haneda, H.; Ohashi, N.; Hishita, S.; Yoshikawa, Y. *Catal. Today* **2004**, *93*, 895.
(6) Li, D.; Haneda, H. *Chemosphere* **2004**, *54*, 1099.
(7) Fuerte, A.; Hernández-Alonso, M. D.; Maira, A. J.; Martínez-Arias, A.; Fernández-García, M.; Conesa, J. C.; Soria, J.; Munuera, G. *J. Catal.* **2002**, *212*, 1.
(8) Ihara, T.; Miyoshi, M.; Iriyama, Y.; Matsumoto, O.; Sugihara, S. *Appl. Catal. B: Environ.* **2003**, *42*, 403.
(9) Irie, H.; Watanaba, Y.; Hashimoto, K. *J. Phys. Chem. B* **2003**, *107*, 5483.
(10) Gole, J. L.; Stout, J. D.; Burda, C.; Lou, Y.; Chen, X. *J. Phys. Chem. B* **2004**, *108*, 1230.
(11) Anpo, M.; Takeuchi, M. *J. Catal.* **2003**, *216*, 505.
(12) Nakamura, I.; Negishi, N.; Kutsuna, S.; Ihara, T.; Sugihara, S.; Takeuchi, K. *J. Mol. Catal. A: Chem.* **2000**, *161*, 205.
(13) Minero, C.; Mariella, G.; Maurino, V.; Pelizzetti, E. *Langmuir* **2000**, *16*, 2632.
(14) Vohra, M. S.; Kim, S.; Choi, W. *J. Photochem. Photobiol. A: Chem.* **2003**, *160*, 55.
(15) Yu, J. C.; Yu, J.; Ho, W.; Jiang, Z.; Zhang, L. *Chem. Mater.* **2002**, *14*, 3808.

10.1021/cm049100k CCC: $30.25
Published on Web 04/19/2005

in these fluorinated or F-doped TiO_2 systems. However, recent study indicates that F-doping in TiO_2 can also induce a visible-light-driven photocatalysis by the creation of oxygen vacancies.[16] In our study, nitrogen and fluorine atoms were simultaneously codoped into the TiO_2 crystal lattice by spray pyrolysis (SP) with the aim of introducing new active sites while the visible-light absorption is improved. As a result, a highly reactive, visible-light-driven photocatalysis would be achieved.

Spray pyrolysis (SP) is a versatile technique for producing ceramic materials on the industrial scale with a wide variety of particle morphologies, sizes, and compositions.[17] In our previous reports, we successfully used SP to prepare N-doped ZnO-based photocatalysts that can work efficiently under visible-light irradiation.[2,5,6] A distinctive feature of these sprayed powders is the homogeneous distribution of constituents throughout all of the particles because all of the constituents are formed from a solution.[18] Utilizing this advantage, we expected that the doped nitrogen and fluorine atoms could be distributed homogeneously throughout the TiO_2 particles, as in the ZnO case.

This paper describes the SP synthesis of NFT powders, and their surface characterization by FE-SEM, XRD, TG-DTA, NH_3-TPD, XPS, and N_2 adsorption analysis. The effects of N−F-codoping on the intrinsic characteristics of TiO_2 are investigated in detail. The mechanism for the formation of the porous NFT powders and the pathways of N- and F-doping are also discussed.

2. Experimental Section

2.1. Synthesis. N−F−codoped TiO_2 (NFT) powders were synthesized by SP from a mixed aqueous solution containing $TiCl_4$ (0.03 M) and NH_4F (0.20 M) as TiO_2 and N/F precursors, respectively. The starting solution was first atomized by a nebulizer; then, the formed droplets passed through a high-temperature tube under the suction of an aspirator. The pyrolysis proceeded quickly as droplets passed through the high-temperature tube. The generated powder was collected with a ceramic filter at the end of the tube. A series of NFT powders was prepared by changing the SP temperature: they were designated as NFT-xxx, where "xxx" represents the SP temperature in °C. For comparison, undoped SP TiO_2 (T-800) and commercial P25 (Degussa, 50 m^2/g, 75% rutile and 25% anatase) were selected as reference samples.

2.2. Characterization. The particle morphology was observed with an Hitachi S-5000 FE-SEM at an acceleration voltage of 10 kV. The XRD pattern was obtained on a Philips PW1800 X-ray diffractometer using Cu Kα radiation with a generator voltage of 40 kV and tube current of 50 mA. The TG-DTA was performed on a TG/DTA6200 system (Seiko Instruments Inc., Japan) in an air atmosphere. Samples were heated from room temperature to 1073 K at 10 K min^{-1}. N_2 adsorption at 77 K was carried out using a BEL-SORP-28SA automatic gas adsorption apparatus (BEL Japan, Inc.).

The XPS measurements were carried out using an ESCALAB 200-X system (VG Scientific) with monochromatic Mg Kα excitation and a charge neutralizer, and all the bonding energies were calibrated to the C 1s peak at 284.8 eV of the surface adventitious carbon. For XPS measurement, all as-sprayed NFT powders (0.30 g) were pretreated under O_2 flow at 673 K for 2 h in order to completely decompose and remove any possible precursor residues and organic contaminants. The calcined powder was pressed into a disk of 7 mm diameter under a pressure of 100 kg/cm^2. Prior to the XPS measurement, the sample was cleaned by an Ar^+ gun. The ion gun settings were as follows: 4 kV, 0.5 $\mu A/cm^2$, incident angle of 60°, and chamber pressure of 9×10^{-5} Pa (Ar). The speed of sputtering was about 3 nm/min in depth.

The NH_3-TPD was conducted using a TPD-1-TA instrument (BEL Japan, Inc.). The sample of 0.100 g was evacuated at 673 K for 1 h, and then the bed temperature was cooled to 373 K. After that, NH_3 (6.4×10^{-4} mol) was introduced, the sample was kept for NH_3 adsorption at 373 K for 0.5 h, and the gaseous NH_3 was then evacuated. The bed temperature was elevated to 1173 K at a rate of 10 K min^{-1}. The desorbed NH_3 was detected by a quadruple mass analyzer.

3. Results and Discussion

3.1. Characterization of the NFT Powders. *3.1.1. Morphology.* The NFT powders were vivid yellow due to N-doping.[1,8−10] The SEM images of selected samples prepared at different SP temperatures are shown in Figure 1. All NFT powders consisted of spherical particles with a porous surface morphology: the particle sizes of the samples were approximately the same, indicating that the SP temperature had little effect on the size and shape of the particles. The undoped T-800 was also in the form of spherical particles, but with a smooth surface morphology. The magnified surface morphologies of some typical particles from NFT-800 are shown in Figure 2. The porous surface could be observed clearly. The structure of the particles consisted of nanosized crystallites. An improvement in adsorptivity for reactants could be expected due to such a unique surface structure.

3.1.2. N_2 Adsorption. The nitrogen adsorption isotherms measured at 77 K on the NFT powders are given in Figure 3. The adsorbed nitrogen amount greatly depended on the SP temperature; the higher the SP temperature, the lower the nitrogen amount of adsorption. All NFT samples show adsorption isotherms of type II in the IUPAC classification.[19] The type II adsorption isotherm is often observed when multimolecular layer adsorption occurs on a nonporous solid. However, the adsorption isotherms of the NFT powders demonstrated a vertical rise at low p/p_0, confirming the presence of micropores in the NFT powders. Then the isotherms were almost linear and finally convex to the p/p_0 axis. It indicates the formation of an adsorbed layer whose thickness increased progressively with increasing the p/p_0. The rapid rise when the p/p_0 closed to 1 means that the adsorbed layer became a bulk liquid or solid.[20] Desorption isotherms (omitted for clarity) of these samples were completely consistent with their corresponding adsorption isotherms, and no hysteresis phenomena were observed, indicating the absence of mesopores in these NFT powders.

(16) Li, D.; Haneda, H.; Hishita, S.; Ohashi,N.; Labhsetwar, N. K. *J. Fluorine Chem.* **2005**, *126*, 69.
(17) Messing, G. L.; Zhang, S.; Jayanthi, G. V. *J. Am. Ceram. Soc.* **1993**, *76* (11), 2707.
(18) Li, D.; Ichikuni, N.; Shimazu, S.; Uematsu, T. *Appl. Catal., A* **1999**, *180*, 227.
(19) Sing, K. S. W.; Everett, D. H.; Haul, R. A. W.; Moscou, L.; Pierotti, R. A.; Rouquerol, J.; Sieminewska, T. *Pure Appl. Chem.* **1985**, *57*, 603.

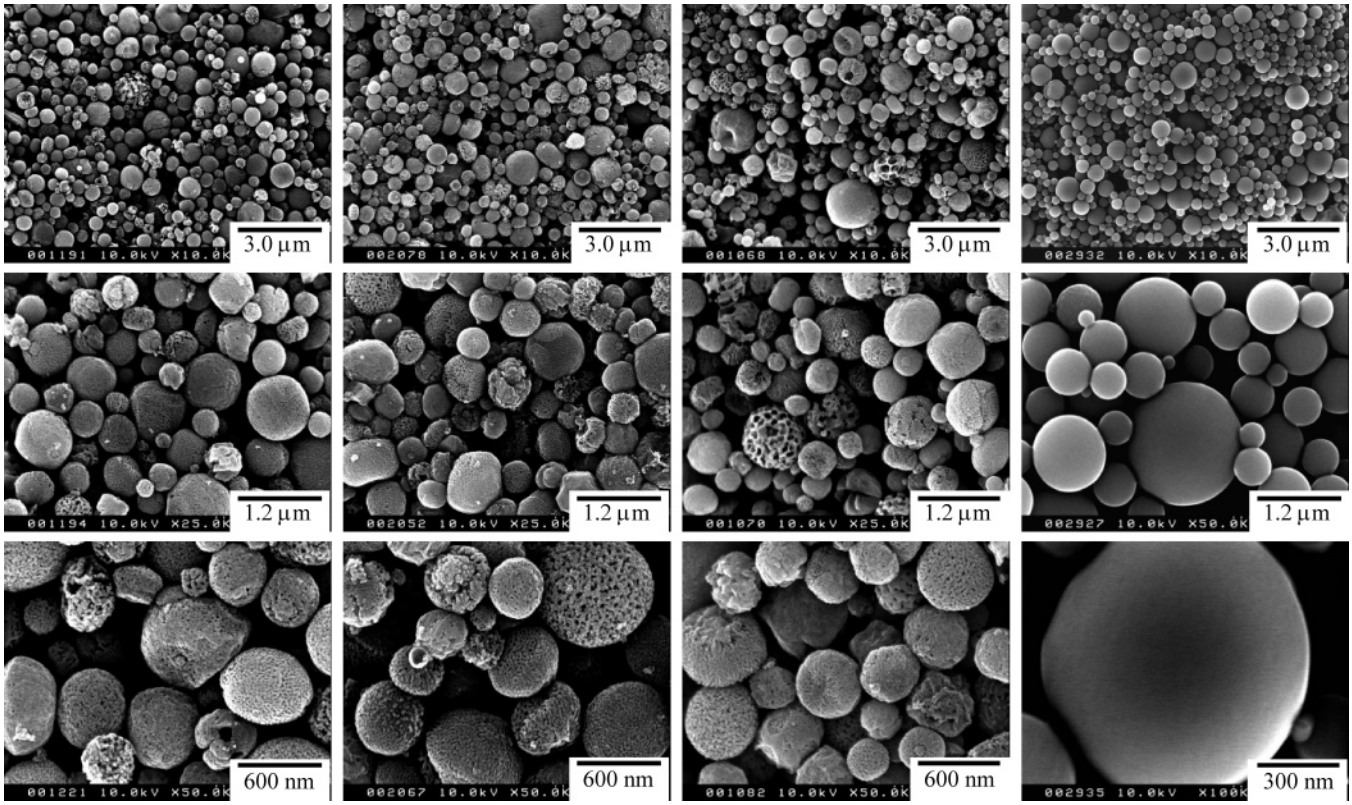

Figure 1. SEM images of NFT powders prepared at different SP temperatures. 1st line pictures were for NFT-600, 2nd line for NFT-800, 3rd line for NFT-1000, and 4th line for T-800.

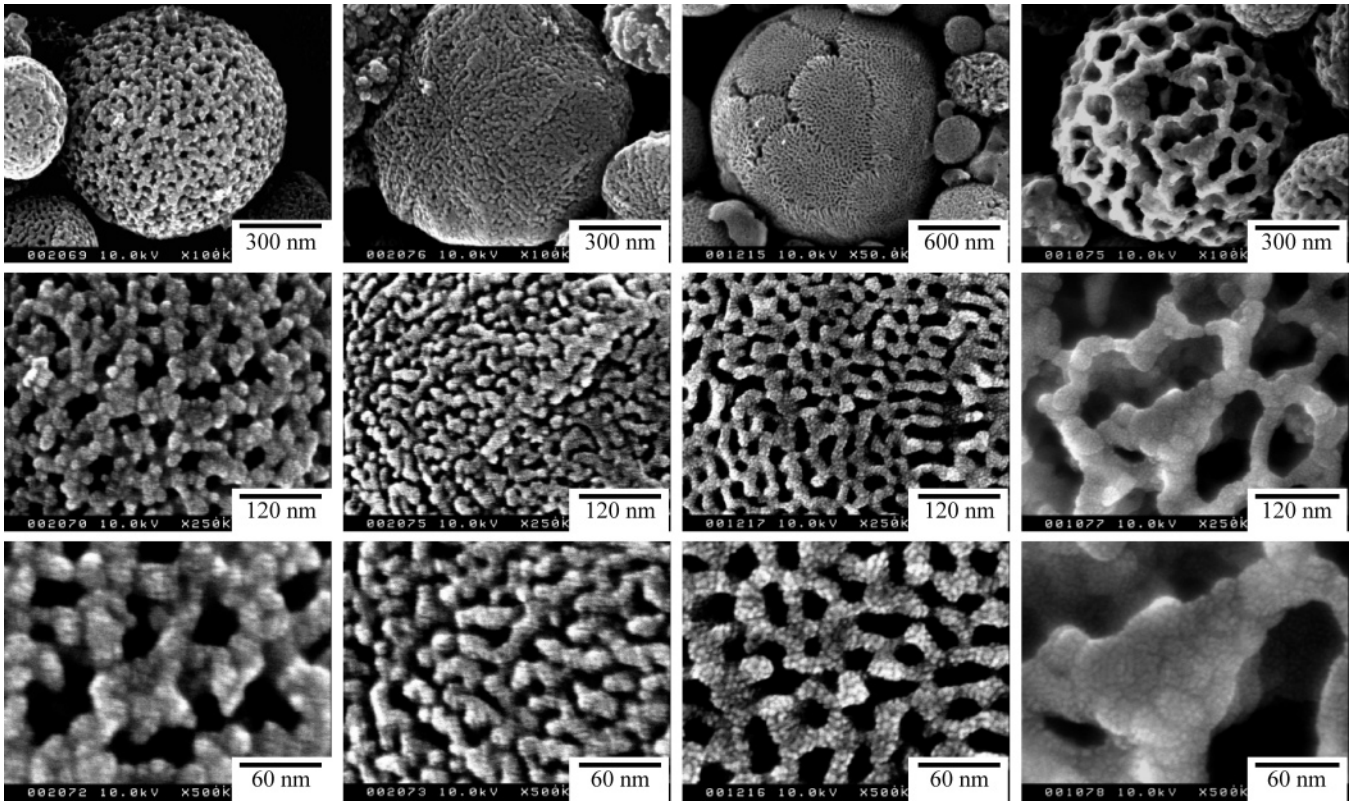

Figure 2. Surface morphologies of some typical particles from NFT-800.

Based on these isotherms, surface and porous structure parameters such as the total surface area (S_{tot}), the interior surface area (S_{int}), and the microporous volume (V_{mp}) could be calculated for all samples by using the *t*-plot method.[20] The results are shown in Figure 4 and Table 1. The V_{mp} of the NFT samples varied from 0.05 to 0.035 mL/g, and S_{tot} (Table 1) was from 44 to 153 m^2/g. The presence of

(20) Rouquerol, F., Rouquerol, J., Sing, K., Eds. *Adsorption by Powders and Porous Solids*; Academic Press: London, 1999.

Table 1. N and F Concentrations and Surface Acid Amounts of NFT Powders

sample	S_{tot} ($m^2\ g^{-1}$)	total-N (at. %)	site-N (at. %)	total-F (at. %)	site-F (at. %)	$TiOF_2$[a] (wt %)	acid site density (μmol m^{-2}) (K)
NFT-500	83.2	0.38	0.08	3.15	0.18	6.06 (5.18[c])[b]	
NFT-600	153.4	1.19	0.21	2.80	0.23	5.20 (5.37)	0.65 (576.1)[d]
NFT-700	135.3	1.22	0.26	2.35	0.27	4.16 (4.08)	0.72 (574.6)
NFT-800	122.7	0.83	0.20	1.90	0.32	3.13 (3.15)	0.79 (573.0)
NFT-900	101.8	0.61	0.18	1.35	0.40	1.85 (1.76)	0.88 (568.2)
NFT-1000	72.9	0.52	0.11	1.01	0.35	1.28 (1.34)	0.81 (556.2)
NFT-1100	43.8	0.44	0.10	0.56	0.11	0.87 (0.93)	0.29 (527.6)

[a] From XPS spectra, based on the phase compositions of $TiOF_2$ and TiO_2. [b] From TG-DTA curves, based on the weight loss between 673 and 873 K. [c] From the calcined NFT-500. [d] NH_3 desorption temperature.

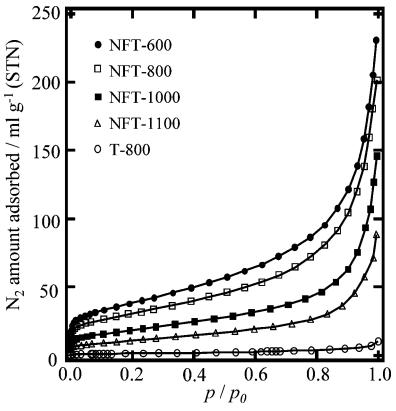

Figure 3. N_2 adsorption isotherms at 77 K on NFT powders.

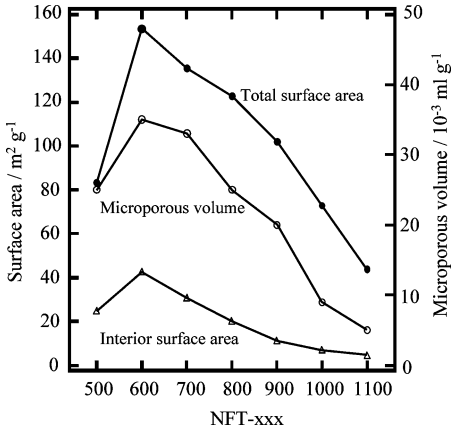

Figure 4. Dependencies of the porous parameters of NFT powders on the SP temperature.

micropores should be important for enhancing the adsorptivity of the NFT powders for reactants since adsorbate molecules always first fill in the micropores that possess a deep potential well.[20,21] The maximum values of V_{mp} and S_{tot} were observed on NFT-600. In the SP process (discussed later), a large amount of rapidly evolving gas is the main reason for the formation of the pores in the particles. The SP at a lower temperature could not meet this condition, whereas a high SP temperature would lead to the collapse of the formed pores. In our case, the 873 K was the optimal SP temperature for the creation of the particle pores. Additionally, the porous structure parameters of the NFT powders were much higher than that of T-800 in which no micropores were observed. The surface area of T-800 was too low (5 m^2/g). Therefore, we can conclude that the introduction of NH_4F in sprayed solution facilitated the formation of porous particles.

(21) Li, D.; Kaneko, K. *J. Phys. Chem. B* **2000**, *104*, 8940.

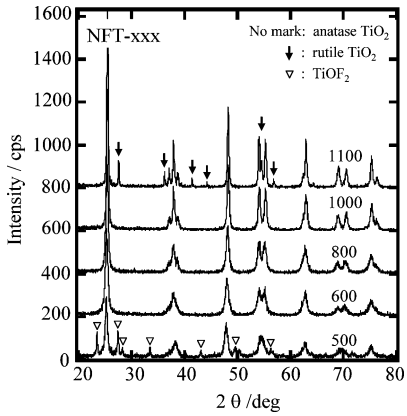

Figure 5. XRD pattern of as-sprayed NFT powders.

3.1.3. Structure. The XRD pattern in Figure 5 indicates that the as-sprayed samples belonged to anatase TiO_2 when the SP temperature ranged from 873 to 1273 K. The rutile phase appeared when the SP temperature was elevated to 1373 K, and some peaks assigned to NH_4Cl were also observed in the NFT-500 since part of NH_4Cl did not decompose during the preparation. NH_4Cl was formed as the $TiCl_4$ and NH_4F precursors were mixed in the starting solution according to reaction 1.

$$TiCl_4 + 6NH_4F = (NH_4)_2TiF_6 + 4NH_4Cl \qquad (1)$$

Additionally, we did not find any shift in the peak position caused by the N−F-codoping. This could be easily understood for the doped F atom because its ion radius (0.133 nm) is virtually the same as that of the replaced oxygen atom (0.132 nm). For the doped N atom, its concentration (given later) might be too low to cause such a shift, although it has a larger ion radius (0.171 nm). Moreover, the crystallite sizes calculated from the (101) peak of the XRD pattern are about 13, 15, 18, and 23 nm corresponding to NFT-600, -800, -1000, and -1100, respectively. These values are almost identical to those of the observed primary particles (Figures 1 and 2).

3.1.4. Thermal Analysis. To fully understand the stability of the NFT powders, we investigated the thermal behavior of the as-sprayed powders. TG-DTA curves for selected samples are shown in Figure 6. A clear exothermic reaction peak at 574 K was observed for NFT-500 and NFT-600. We assigned this peak to the decomposition of the residual NH_4Cl. Both the XRD pattern of the NFT-500 and the TG-DTA curve of the NH_4Cl (Figure 10) strongly support this conclusion. Based on their weight loss, the residual amount of the NH_4Cl was calculated as 12.7% for NFT-500 and

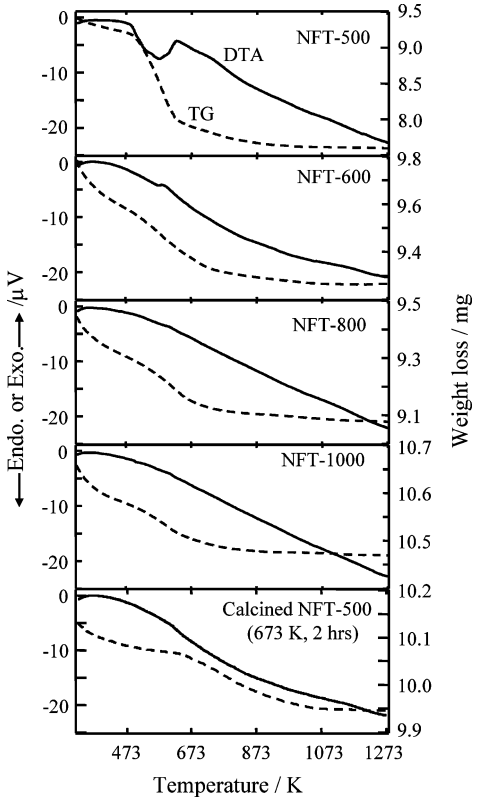

Figure 6. TG-DTA curves of selected NFT powders.

2.16% for NFT-600, indicating that the residual amount of NH_4Cl rapidly decreased with SP temperature. However, some NH_4Cl residue was still detected in the weight loss of the TG curve even for the NFT-1000 sample prepared at the SP temperature of 1273 K, although no exothermic peaks were found in its DTA curve. Assuming that the weight loss between 473 and 673 K is attributed to the residual NH_4Cl decomposition, the residual NH_4Cl amount was found to be approximately 1.95%, 1.68%, 0.98%, 0.71%, and 0.52% for NFT-700, -800, -900, -1000, and -1100, respectively. The residual NH_4Cl in the NFT powders could be removed by calcinations; a weight loss corresponding to the NH_4Cl was not observed for NFT-500 calcined at 673 K for 2 h in air (Figure 6). Additionally, a weight loss was observed between 673 and 1073 K for each sample. This was ascribed to the decomposition of the $TiOF_2$ and would be discussed in the next section.

3.1.5. Chemical Forms of the N and F Atoms in the NFT Powders. The chemical forms and concentrations of the N/F atoms in the NFT powders were investigated from the analysis of XPS spectra. Figure 7a shows the N_{1s} XPS spectra of NFT-900 before and after Ar^+ sputtering with different times. In the spectrum before sputtering, only a broad peak appeared at 400.0 eV. This peak was ascribed to the N atoms from *adventitious* N_2, NH_3, or N-containing organic compounds adsorbed on the surface.[22−24] However, this peak was still present after sputtering. Therefore, we ascribed the peak that remained after sputtering to the *native* N atoms adsorbed

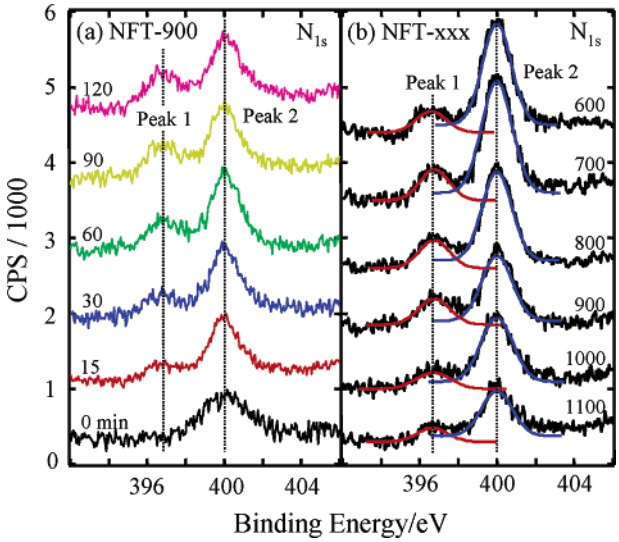

Figure 7. N_{1s} XPS spectra: (a) for NFT-900 before and after Ar^+ sputtering with different times; (b) for NFT powders after 60 min Ar^+ sputtering.

on the surface of exposed particle boundaries, primary particles, or originally closed pores in the NFT powders. This conclusion was inferred from the following: (1) the adventitious C peak (omitted for clarity) was not observed after 30 min sputtering, indicating that the contaminants presented on the surface before sputtering were removed completely; (2) the total-N concentrations calculated from the XPS spectra (e.g., 1.22 at. % for NFT-700) were very close to the values obtained from elemental analysis (e.g., 1.08 at. % for NFT-700). After sputtering for 15 min, a new peak was observed at 396. 6 eV. This peak is generally considered as the evidence for the presence of Ti−N bonds formed when the N atoms replace the oxygen in the TiO_2 crystal lattice.[1,9,22] Here, these N atoms are called site-N. Also, the intensity of both peaks did not vary with an increase of the sputtering time after 30 min, indicating two kinds of N species were distributed homogeneously throughout the particles.

The N_{1s} XPS spectra of all NFT powders after 60 min of Ar^+ sputtering are shown in Figure 7b. The deconvolution of two peaks is also given there. Based on these XPS spectra, N concentrations in the NFT powders were calculated and summarized in Table 1. The site-N concentrations in the NFT powders depended on the SP temperature and ranged from 0.10 to 0.26 at. %. The maximum concentration of site-N was observed for NFT-700.

Figure 8a gives the F_{1s} XPS spectra of the NFT powders after 60 min of Ar^+ sputtering. A tailing F_{1s} peak was found for the NFT powders prepared at low SP temperature, and two peaks was found for the NFT powders prepared at high temperature. This infers that two chemical forms of F atoms may exist in the NFT powders. So far, less information was reported on the XPS spectra of the F atoms doped into TiO_2.[15] Therefore, to elucidate the origin of the two chemical forms of the F atoms in the NFT powders, a pure $TiOF_2$ powder was prepared by treating TiO_2 with HF aqueous solution in a Pt crucible.[25] The as-prepared $TiOF_2$ powder was calcined at different temperatures for 4 h in air. The calcined $TiOF_2$ powders were denoted as $TiOF_2$-200, -400, -500, and -600,

(22) Saha, N. C.; Tompkins, H. G. *J. Appl. Phys.* **1992**, *72*, 3072.
(23) Lazarus, M. S.; Sham, T. K. *Chem. Phys. Lett.* **1982**, *92*, 670.
(24) Wagner, C. D.; Riggs, W. M.; Davis, L. E.; Moulder, J. F. *Handbook of X-ray Photoelectron Spectroscopy*; Muilenberg, G. E., Ed.; Perkin-Elmer Co., Minnesota, 1979.

(25) Vorres, K. S.; Dutton, F. B. *J. Am. Chem. Soc.* **1955**, *77*, 2019.

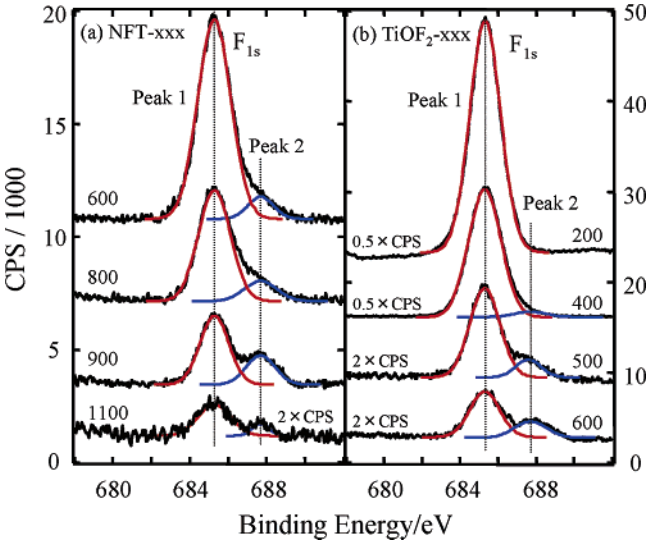

Figure 8. F_{1s} XPS spectra: (a) for NFT powders after 60 min Ar^+ sputtering; (b) for $TiOF_2$ powders calcined at different temperatures. The phase compositions by XRD were $TiOF_2$, $TiOF_2$−anatase TiO_2, anatase TiO_2, and anatase−rutile TiO_2 for $TiOF_2$-200, -400, -500, and -600, respectively.

where the numbers represent the calcination temperature in °C. The reason for the selection of $TiOF_2$ was based on a fact that $TiOF_2$ seems to be the only stable phase presented during TiO_2 preparation when the F-containing compounds (e.g., TiF_4, H_2TiF_6, and $(NH_4)_2TiOF_4$) were used as TiO_2 precursors.[16,26,27] The F_{1s} XPS spectra of these calcined $TiOF_2$ powders (Figure 8b) were investigated under completely identical conditions with the NFT powders. A well symmetrical F_{1s} peak at 685.3 eV was observed for $TiOF_2$-200, which contained pure $TiOF_2$ phase. However, a new peak appeared with an increase of the calcination temperature, indicating that part of the F atoms from $TiOF_2$ transferred into different chemical form. Therefore, the F_{1s} peak of each calcined $TiOF_2$ powder except $TiOF_2$-200 was deconvoluted into two separate peaks with Gaussian distributions. Obviously, the peak 1 located at 685.3 eV is originated from the F atoms of the $TiOF_2$. However, the peak 2 located at 687.6 eV was attributed to the doped F atoms in TiO_2, i.e., the substitutional F atoms that occupied oxygen sites in the TiO_2 crystal lattice. This conclusion was based on two facts: (1) the formation of TiO_2 by the calcination of $TiOF_2$ proceeds by the substitution of oxygen atoms for F atoms and also it is reasonable to assume that some of the Ti−F bonds in the $TiOF_2$ do not break and remain in the TiO_2 crystal lattice; (2) the position of the peak 2 was close to the value reported by Yu for the substitutional F atoms in TiO_2.[15]

Based on the XPS results of the $TiOF_2$, it is easy to elucidate the two chemical forms of F atoms in the NFT powders. The F_{1s} peak of each sample in Figure 8a was also deconvoluted into two separate peaks as in the case of the $TiOF_2$ powders. The positions of peak 1 (685.3 eV) and peak 2 (687.8 eV) completely agreed with those of the F atoms from the calcined $TiOF_2$ powders. This result indicates that

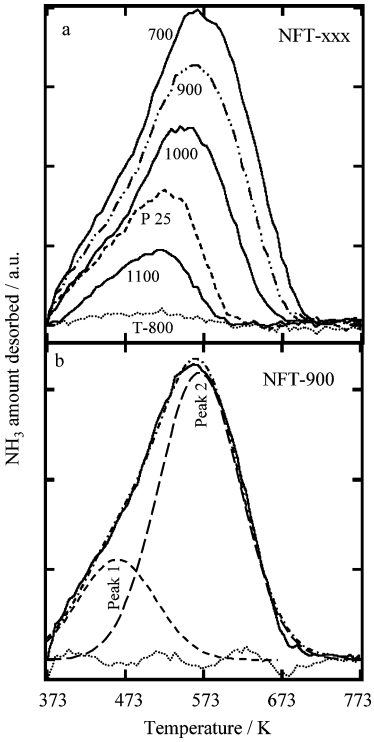

Figure 9. (a) NH_3-TPD profiles of NFT powders. (b) The deconvolution of NH_3 desorption peak for NFT-900. The dotted line in Figure 9b represents the error of the fitting.

a part of the F atoms in the NFT powders existed in the form of the $TiOF_2$ and the other part was doped F atoms (site-F). The concentrations of the total-F and site-F atoms in the NFT powders are listed in Table 1. The site-F concentrations ranged from 0.11 to 0.40 at. %; its maximum value was observed in the NFT-900. The amount of the doped F atoms in the NFT powders is greater than that of the N atoms. This indicates that F atoms are easily doped into oxygen sites of the TiO_2 crystal lattice compared to N atoms. This could be ascribed to the difference in their ion sizes, as mentioned above, as well as to the different doping mechanism as discussed later.

Additionally, it is worth noting that most of the F atoms in the NFT powders were in the form of $TiOF_2$. The contents of $TiOF_2$ derived from XPS data in each NFT powder is listed in Table 1; they ranged from 0.87 to 6.06 wt %. As mentioned above, a weight loss was observed between 673 and 1073 K in the TG curves for each NFT powder. Based on these weight losses, the wt % of the $TiOF_2$ in the NFT powders was also calculated (Table 1) for comparison. A good agreement was observed in both methods: XPS spectra and TG-DTA curves, indicating that the $TiOF_2$ decomposition was really responsible for the weight losses between 673 and 1073 K.

3.1.6. NH_3-TPD. The surface acidity of a photocatalyst has a great effect on its photocatalytic activity.[28,29] Therefore, the adsorbed NH_3 amount on the NFT powders was investigated by NH_3-TPD measurement. The results are shown in Figure 9a. The NH_3 desorption profile, a broad

(26) Lytle, J. C.; Yan, H.; Turgeon, R. T.; Stein, A. *Chem. Mater.* **2004**, *16*, 3829.
(27) Laptash, N. M.; Merkulov, E. B.; Maslennikova, I. G. *J. Therm. Anal. Calorim.* **2001**, *63*, 197.
(28) Martra, G. *Appl. Catal., A* **2000**, *200*, 275.
(29) Kwon, Y. T.; Song, K. Y.; Lee, W. I.; Choi, G. J.; Do, Y. R. *J. Catal.* **2000**, *191*, 192.

peak, depended on the SP temperature. Less NH_3 desorption was observed for T-800, indicating that the N−F-codoping greatly increased the surface acidity of TiO_2. Each profile was deconvoluted into two peaks with Gaussian distributions. The deconvolution for the NFT-900 sample is given in Figure 9b. In this study, the first peak at 463 K was attributed to the NH_3 weak adsorption; the second peak was attributed to the NH_3 adsorption on the acid sites. Therefore, the acid site amount corresponding to the second peak and the desorption temperature were used to represent the acidities of the NFT powders (Table 1). The NFT powders demonstrated a strong acidity when the SP temperature was less than 1273 K. It was higher than that of P25 (0.68 μmol g^{-1}) no matter how the acid amount was represented: per square meter or per gram. The acidity of the NFT powders was attributed to the contained F atoms because we found that F introduction significantly increased the acidity on the surface of TiO_2 and only N-doping almost had no effect.[16,30] As for the structure of the acid sites, Lewis or Brønsted acid site, further experiments are needed for the NFT powders. In general, pure anatase TiO_2 shows only the Lewis acidity, and does not demonstrate the Brønsted acidity.[31]

3.2. Formation Mechanism of the NFT Powders. *3.2.1. Formation of Porous Particles.* The SP process generally involves several stages: atomization, solvent evaporation and solute precipitation, drying, precursor decomposition, calcinations, and particle shaping.[17] The physical and chemical properties of the precursors, e.g., thermostability, solubility, and diffusion rate in the solvent used, govern the distribution of every component in a particle.[32] Gas evolution that occurred during the formation of particles determines the final shape and surface morphology of the particles.[33]

In the case of the NFT powders, the starting solution contained three components, $(NH_4)_2TiF_6$, NH_4F, and NH_4Cl (reaction 1), and a high concentration of NH_4F was used to increase the N−F-codoping and to produce a large amount of gas to promote the formation of porous particles. Therefore, thermal decomposition behaviors of NH_4F and NH_4Cl and the hydrolysis characteristics of $(NH_4)_2TiF_6$ should have a great influence on the particle morphology. Figure 10 shows the TG-DTA curves for NH_4F, NH_4Cl, and NFT-100. We found that the decomposition temperatures of NH_4F and NH_4Cl were different: ranging from 433 to 523 K for NH_4F and 478−618 K for NH_4Cl. The first peaks in Figures 10a and 10b were assigned to the endothermic melting peak of NH_4F and the dehydration endothermic peak of NH_4Cl, respectively. Moreover, NH_4F is easy to decompose into NH_3 and HF in water; it can never separate out when an NH_4F aqueous solution is heated.[34a]

$(NH_4)_2TiF_6$ is unstable even in air and its hydrolysis occurs easily in water.[34b] Here, to confirm that the TiO_2 particles

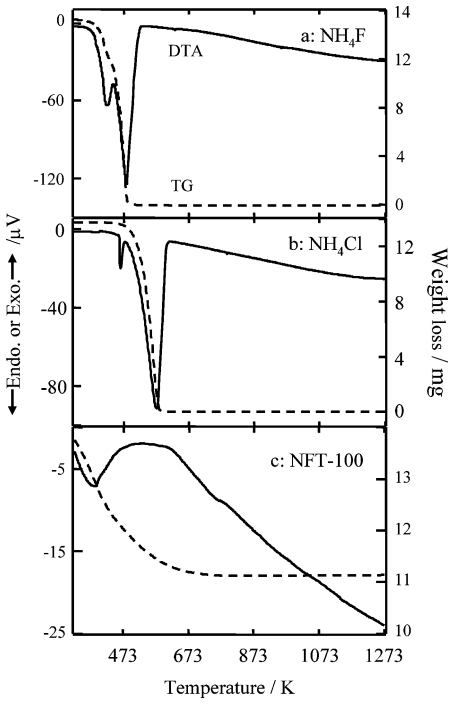

Figure 10. TG-DTA curves of NH_4F, NH_4Cl, and NFT-100.

had formed within the droplets before water evaporation, we lowered the SP temperature to 373 K and tried to prepare an NFT-100 sample. As a result, we obtained a watery white powder. After water washing and vacuum-drying of the sample at 333 K for 24 h, the XRD measurement was carried out. The result indicated that it was anatase TiO_2 powder with a very poor crystallinity. The TG-DTA (Figure 10c) also indicated that it only contained water molecules. Its crystallization began at 473 K and ended at 673 K.

Based on these results, we proposed a mechanism for particle formation in the SP process, as shown in Figure 11. The hydrolysis of $(NH_4)_2TiF_6$ into hydrous TiO_2 and decomposition of NH_4F into gaseous NH_3 and HF proceeded simultaneously in a heated droplet. The enormous gas evolution from the NH_4F decomposition, as well as the $(NH_4)_2TiF_6$ hydrolysis, promoted the formation of a porous particle of TiO_2. Afterward, the pores on/in the particles were filled with NH_4Cl produced with the water evaporation in droplets. This speculation is supported by the NH_4Cl diffraction peaks (Figure 5) of the NFT-500. The sediment NH_4Cl itself played a role of a template which prevented the collapse of the porous structure during TiO_2 drying and crystallization. Moreover, enormous NH_3 and HCl gas evolution from the NH_4Cl decomposition not only led to the formation of new pores in the TiO_2 particles but also prevented the originally formed pores from collapse. Therefore, the pores initially formed during the $(NH_4)_2TiF_6$ hydrolysis stage were maintained until the last stage. Accordingly, porous particles were obtained for the NFT powder. The coincidence of $(NH_4)_2TiF_6$ hydrolysis and enormous gas evolution from the NH_4F is vital for the formation of porous particles.

For the case of undoped TiO_2, only one component ($TiCl_4$) presented in the starting solution. Therefore, $TiCl_4$ hydrolysis was a vital step for particle formation. Many studies have confirmed that $TiCl_4$ hydrolysis into TiO_2 can proceed easily

(30) Li, D.; Haneda, H.; Hishita, S.; Ohashi, N. *Mater. Sci. Eng. B* **2005**, *117*, 67.
(31) Busca, G.; Saussey, H.; Saur, O.; Lavalley, J. C.; Lorenzelli, V. *Appl. Catal.* **1985**, *14*, 245.
(32) Kim, S. H.; Liu, B. Y. H.; Zachariah, M. R. *Chem. Mater.* **2003**, *14* (7), 2889.
(33) Kieda, N.; Messing, G. L. *J. Mater. Sci. Lett.* **1998**, *17*, 299.
(34) Mizushima, S., Ed. *Encyclopaedia Chimica*; Kyoritsu Publication Co., Ltd., 1989; a: Vol. 7, p 853; b: Vol. 7, p 283.

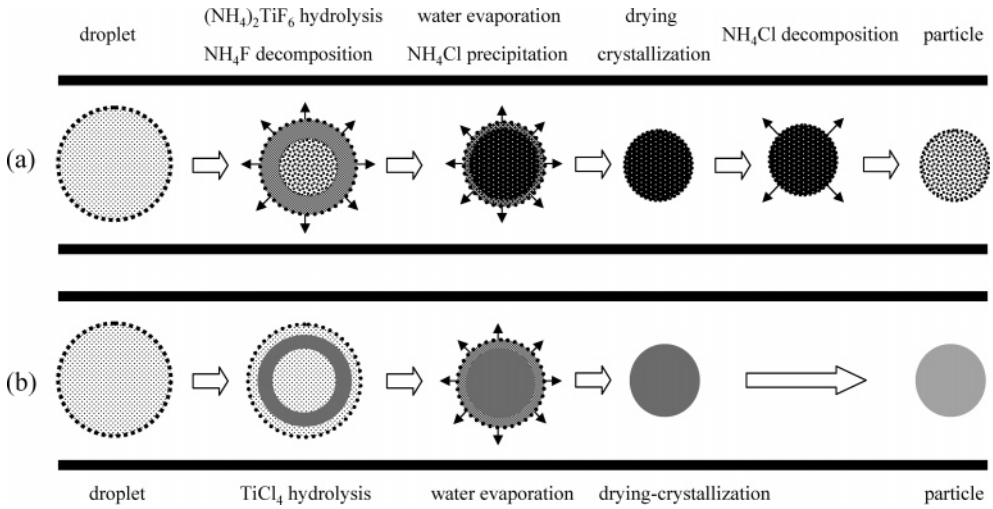

Figure 11. Schematic of the formation of a particle within the pyrolysis tube during the SP process. (a) For a porous NFT particle; (b) for a smooth T-800 particle.

in a heated aqueous solution.[35] When the droplets passed through the tube, the temperature around the droplets gradually increased. $TiCl_4$ hydrolysis proceeded within the droplets and TiO_2 was formed and separated out. TiO_2 precipitation began from the outer layer of a droplet and gradually extended to the center of the droplet so that a dense spherical particle was formed with the water evaporation due to the absence of gas evolution. Next, the particle underwent drying and crystallization, and finally a particle with a smooth surface was obtained because only the vapor from residual water was given off during the crystallization.

3.2.2. Processes of N- and F-Doping. Different mechanisms of the N- and F-doping were considered. The N-doping into the TiO_2 crystal lattice occurred following the NH_4Cl decomposition into NH_3 and proceeded through the reaction 2. The fact that low-level N-doping was observed for NFT-500 indicates that the NH_4Cl decomposition was extremely important for N-doping.

$$TiO_2 + NH_3 \rightarrow TiO_{2-x}N_x + H_2O \qquad (2)$$

The F-doping underwent two pathways: the first one is that part of the Ti−F bonds did not break during the $(NH_4)_2TiF_6$ hydrolysis and directly remained in the TiO_2 crystal lattice. This process is represented by reaction 3. The second one is associated with the decomposition of the high-dispersed $TiOF_2$. The presence of the separate $TiOF_2$ phase in the NFT powders was confirmed by the XPS spectra. The uncompleted decomposition of the $TiOF_2$ led to some of the Ti−F bonds left in the TiO_2 crystal lattice, as shown in reaction 4. Alternatively, the F atoms formed during the $TiOF_2$ decomposition could directly substitute oxygen atoms in the TiO_2 crystal lattice. The F-doping in the NFT powders prepared at low SP temperature proceeded mainly by the first pathway because a higher temperature was needed for the $TiOF_2$ decomposition (Figure 6). The F-doping in the NFT powders prepared at high SP temperature proceeded by both pathways.

$$(NH_4)_2TiF_6 + H_2O \rightarrow TiO_{2-y}F_y + HF + NH_3 \qquad (3)$$

$$TiOF_2 + O_2 \rightarrow TiO_{2-y}F_y \qquad (4)$$

4. Conclusions

We have demonstrated the feasibility of the spray pyrolysis technique in preparing N−F−codoped TiO_2 powders with a porous and acidic surface. The doped N/F concentrations in the NFT powders could be controlled by adjusting the SP temperature and ranged from 0.10 to 0.26 and from 0.11 to 0.40 at. %, respectively. The mechanism for the formation of the porous particle morphology of the NFT powders was ascribed to the enormous gas evolution from the NH_4F during the TiO_2 particle formation and the template role played by the NH_4Cl.

Acknowledgment. This research is part of the Millennium Project for the "Search and Creation of a Catalyst for Removing Harmful Chemical Substances" sponsored by the Ministry of Education, Culture, Sports, Science and Technology (MEXT), Japan. It was also supported by the Industrial Technology Grant Program (ID04A26018) from New Energy and Industrial Technology Development Organization (NEDO), Japan. Here, we are grateful for the financial support.

CM049100K

(35) Zhang, Q.; Gao, L.; Guo, J. *NanoStruct. Mater.* **1999**, *11* (8), 1293.